Evaluation of a fast single-photon avalanche photodiode for measurement of early transmitted photons through diffusive media

Ying Mu, Niksa Valim, and Mark Niedre*

Department of Electrical and Computer Engineering, Northeastern University, Boston, Massachusetts 02115, USA
**Corresponding author: mniedre@ece.neu.edu*

Received March 20, 2013; revised May 13, 2013; accepted May 13, 2013;
posted May 15, 2013 (Doc. ID 187452); published June 10, 2013

We tested the performance of a fast single-photon avalanche photodiode (SPAD) in measurement of early transmitted photons through diffusive media. In combination with a femtosecond titanium:sapphire laser, the overall instrument temporal response time was 59 ps. Using two experimental models, we showed that the SPAD allowed measurement of photon-density sensitivity functions that were approximately 65% narrower than the ungated continuous wave case at very early times. This exceeds the performance that we have previously achieved with photomultiplier-tube-based systems and approaches the theoretical maximum predicted by time-resolved Monte Carlo simulations. © 2013 Optical Society of America

OCIS codes: (170.6920) Time-resolved imaging; (110.0113) Imaging through turbid media; (110.6955) Tomographic imaging.
http://dx.doi.org/10.1364/OL.38.002098

The high degree of photon scatter through biological tissue is a persistent problem and is the primary cause of the relatively poor imaging resolution in diffuse optical tomography (DOT) and fluorescence-mediated tomography (FMT) [1]. Time-resolved (TR) measurement of early-transmitted photons from a pulsed laser has been studied as a method for improving this limitation by a number of groups [2–5]. The concept is that the earliest photons arriving at a detector from a pulsed laser have experienced fewer total average scattering events and have taken relatively less diffuse paths. In practice, this has been shown to reduce the width of the photon-density sensitivity function [(PDSF), or "Jacobian"] between a source and detector pair, resulting in a better conditioned inverse problem and improved imaging resolution.

In recent years, our group has also studied the "early photon" (EP) effect in some detail and showed that the relative reduction in PDSF width is dependant not only on the time on the rising edge of the transmitted TR curve and the optical properties of the media but also on the characteristics of the TR instrument itself [6]. Of particular importance to the present work, we recently showed both experimentally and by analysis of TR Monte Carlo (TR-MC) simulations that the measured PDSF full width at half-maximum (FWHM) broadened by about 5% per 100 ps of instrument temporal impulse response function (TIRF) relative to that predicted by TR-MC at early times [6]. Since typical reported instrument TIRFs for TR systems are in the range of 150–500 ps, this has significant impact on the quality of EP measurements. These data also implied that *faster* instruments would provide better EP performance relative to the theoretical maximum, although we were not able to experimentally verify this previously. This led us to consider and test alternative fast detectors for this purpose. In this work we tested a fast single-photon avalanche photodiode [(SPAD); ID-100-50; ID Quantique, Geneva, Switzerland]. Although SPADs have been used in a small number of DOT and FMT systems previously—for instance [7,8]—to our knowledge they have never been systematically characterized in measurement of EPs to improve resolution previously. In this context, SPADs have a number of potential advantages including a rapid response time in the range of 30–40 ps, high quantum efficiency, relatively low cost, and high tolerance to damage from direct illumination versus, for example, photomultiplier tubes (PMTs) or multichannel plates (MCPs).

Experimental setup. The system used for these experiments is shown in Fig. 1(a). We used a femtosecond titanium:sapphire laser (MaiTai XF-1, Newport Corporation, Irvine, CA) operating at 730 nm and fitted with a variable attenuator (VA) so that the incident power at the sample was set to 10 mW. Transmitted light from the sample was measured with the SPAD, which was fitted

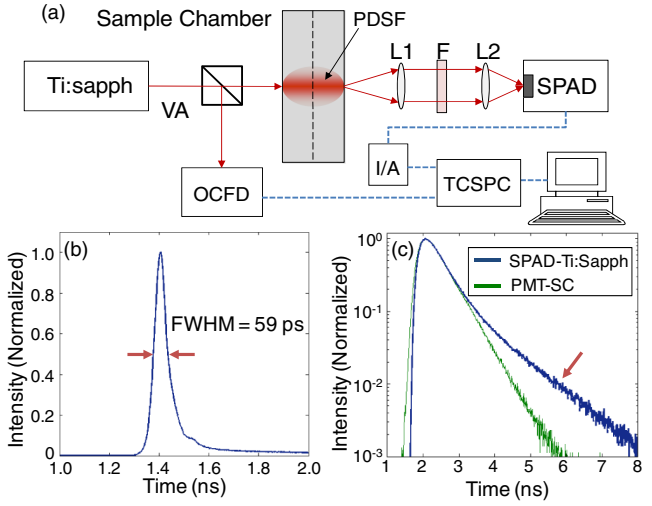

Fig. 1. (a) Schematic of the experimental system used for evaluation of SPAD detector in measurement of EPs. Abbreviations: lens 1,2 (L1, L2), filter (F), inverter and attenuator (I/A), variable attenuator (VA). (b) Measured instrument TIRF. (c) Measured TR curve through diffusive liquid phantom. The SPAD diffusion tail is evident (arrow, blue curve) compared to the TR curve measured with a PMT through the same media (see text).

with a 1 mm aperture, a lens pair ($f = 25$ mm, Edmund Optics), and a 730 nm bandpass filter (Chroma Technology, Belmont Falls, VT). The SPAD produced a +2 V pulse for each measured photon, which was inverted and attenuated (26 dB) before coupling into a time-correlated single-photon counting module (SPC-130; Boston Electronics, Brookline, MA). The measurement was synchronized to the laser pulse using an optical constant fraction discriminator (OCFD).

We first measured the instrument TIRF by placing a thin glass diffusing target in the path of the beam. As shown in Fig. 1(b) the overall TIRF FWHM was 59 ps. This is in good agreement with the manufacturer's specified response time of the SPAD (40 ps) and the timing jitter on the laser (20 ps). This is also significantly faster than the instrument configuration in our previous work [6] and faster than previously reported instruments from other groups that used, for example, fast PMTs, streak cameras, gated intensified CCDs, or multianode-MCP detectors, where stated TIRFs were in the range of 150–500 ps [2–4].

We next replaced the diffusing target with a 2 cm × 20 cm × 20 cm plexiglass imaging chamber (2 cm depth) filled with a homogenous liquid phantom solution with intralipid (1%; Baxter Healthcare) and India ink (50 ppm) added. Based on previously published characterization of similar phantoms at 730 nm we estimated that the resulting optical properties in the media were $\mu_s' = 10$ cm^{-1} and $\mu_a = 0.1$ cm^{-1}, which are close to reported values for biological tissue in this wavelength region [9]. The measured TR curve is shown in Fig 1(c), along with a TR curve measured with our previously described instrument [6] that used a multianode PMT and supercontinuum (SC) laser combination and had an overall TIRF FWHM of 163 ps. As shown, the SPAD TR curve has an extended decay portion compared to the PMT system (red arrow). This is a well-known effect and is caused by carrier diffusion processes in the SPAD material [8]. Therefore, for any application where the full-time curve is of interest, such as in TR measurement of optical properties or fluorescence lifetimes, this effect must be considered, for example by deconvolution of the instrument response function from the TR signal, by using fast time-gated detection approaches as in [8], or by selection of a fluorophore with a long lifetime relative to the diffusion kinetics,

Photon density sensitivity function measurements. We next measured the width of the PDSF through the diffusive media using a technique we have described in detail previously [7]. Briefly, we translated a thin, 10 cm× 10 cm absorbing sheet with a 1 mm wide × 5 cm long slit aperture through the center plane [Fig. 1(a)] of the imaging chamber using a motorized translation stage (XSlide, Velmex Inc., Bloomfield, New York) and measured the TR curve at each point. By analyzing the effect of the slit position on the TR curve we were able to measure the PDSF at its widest point (i.e., in the middle of the chamber). Each measurement took 1 s, and the photon count rate was approximately 10^6 photons/s at maximum. The early portion of an example TR curve is shown in Fig. 2(a), along with the measured normalized PDSF profile at the center of the chamber [Fig. 2(b)] for selected time points [red arrows, Fig. 2(a)]. The average of three experimental trials is shown for each curve. As expected, the width of the PDSF increased at later times due to photon diffusion. The FWHM of the PDSF as a function of time is shown in Fig. 2(c), and the dotted line indicates the width of the time-integrated, quasi-CW PDSF, which in this case was 8 mm. Overall, the rapid TIRF of the system allowed measurement of very narrow PDSFs on the order of 2–3 mm FWHM; this corresponds to a reduction by about 68% compared to quasi-CW. For comparison, we plotted the relative PDSF FWHM obtained with the SPAD along with data obtained from TR-MC simulations for the same geometry as we have done previously [6]. Here we assumed $g = 0.85$, $\mu_s = 67$ cm^{-1}, and $\mu_a = 0.1$ cm^{-1}. For comparison, we also plotted the corresponding curve measured with our previous system that used an SC source and multianode PMT [6] that had an overall TIRF FWHM of 163 ps. To permit direct comparison of systems with different TIRFs, the time axis of these curves were normalized to "fraction of the peak" on the rising edge of the curve. As shown, the SPAD system (with the Ti:sapphire laser) resulted in significantly better performance than our previous system, particularly at very early times. For example, at 1% of peak, the SPAD system was 27% narrower than the PMT system and was extremely close to the theoretical TR-MC performance.

Cylindrical phantom measurement. As a second test of the performance of the SPAD in measurement of EPs, we replaced the chamber with the 25 mm diameter × 100 mm long resin cylindrical phantom (as above, with optical properties approximately equal to $\mu_s' = 10$ cm^{-1} and $\mu_a = 0.1$ cm^{-1}) with two 2 mm diameter bore holes separated by 7 mm center to center as shown in Fig. 3(a). The holes were filled with an absorbing medium with an

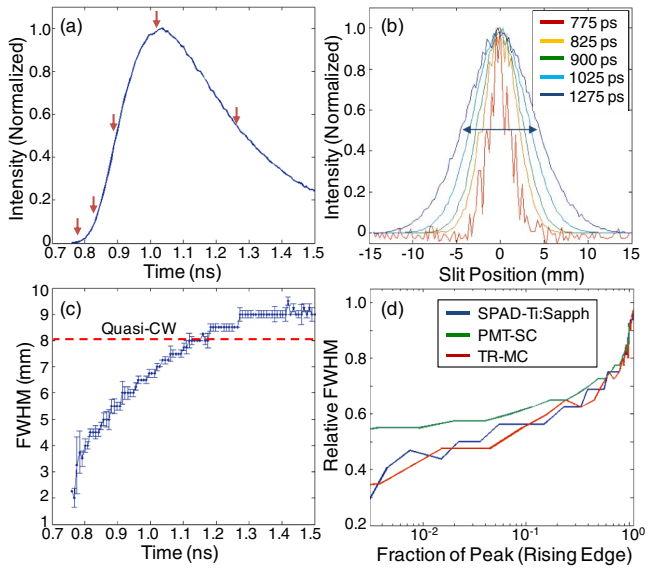

Fig. 2. (a) Measured TR curve through liquid phantom. (b) Measured PDSF profile in the center of the imaging chamber at five time points corresponding to the red arrows in (a), illustrating increasing photon scatter with time. (c) PDSF FWHM versus time. Error bars represent the standard deviation from three trials. (d) The relative PDSF FWHM (normalized to quasi-CW) as a function of time on the rising edge of the TR curve (normalized to fraction of peak) measured with the SPAD and obtained with TR-MC simulations. For comparison, the same curve measured with a PMT (TIRF FWHM = 163 ps) is shown.

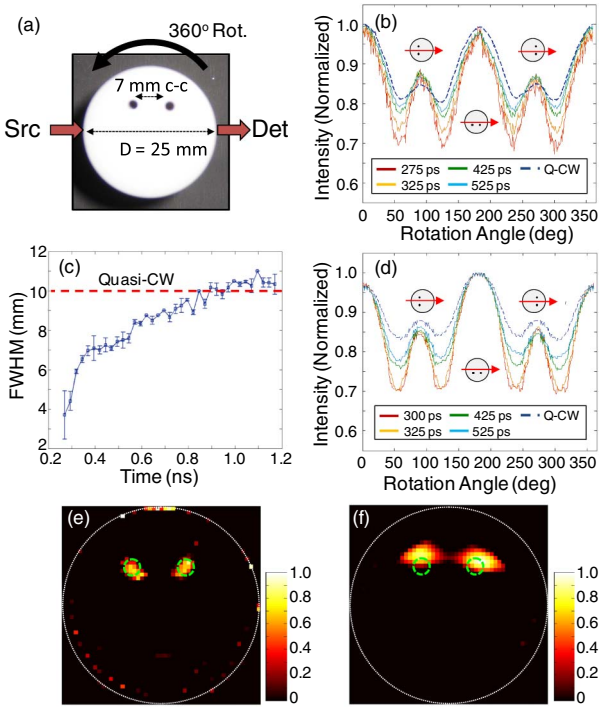

Fig. 3. (a) Cylindrical cast resin phantom with two absorbing inclusions. (b) Normalized measured intensity as a function of rotation angle for four time points along with quasi-CW data. (c) FWHM of PDSFs functions computed with TR-MC at the midplane of the phantom. (d) Simulated TR forward data, analogous to experimental measurements in (c). Example tomographic axial slice reconstructions of attenuation (normalized) are shown for (e) early (to 350 ps) and (f) quasi-CW data. The improved localization and separation of the targets (green dotted circles) with EPs is evident.

estimated absorption coefficient of 3.5 cm^{-1}. The phantom was rotated counterclockwise through 360° with 2° increments using a motorized rotation stage (Velmex), and the transmitted TR curve was measured. Example traces for selected time points along the early portion of the TR curve (corresponding to approximately 1%, 5%, 25%, and 50% of peak) are shown in Fig. 3(b), as well as the quasi-CW measurements. Intensities at each time point were normalized to the maximum value of the scan, and the data shown is the average of three experimental trials. The reduced scatter of EPs is clear in the depth of the attenuation as the absorbers moved directly in front of the laser or detector and the extent of recovery as the gap between the holes passed in front of the laser or detector.

We simulated PDSFs using TR-MC for the phantom geometry, and the FWHM in the middle of the phantom is shown in Fig. 3(c) as a function of time. For comparison we computed the corresponding forward data using a linear model, $y = W \cdot [\mu_{a0} + \delta\mu_a(r)]$, where W was the "weight matrix" of TR-MC computed PDSFs, μ_{a0} was the background absorption, and $\delta\mu_a(r)$ was the absorption due to the inclusions, and the results are shown in Fig 3(d). Generally the agreement with the experimental data was excellent. By analysis of Figs. 3(b)–3(d), we determined the earliest experimentally measured EPs represented a reduction in PDSF width by about 63% compared to CW data. This result is in good agreement with the experiments in Fig. 2 and, as above, represents a significant improvement versus our previous work. Finally, we performed tomographic image reconstructions of attenuation for early (to 350 ps) and quasi-CW data as shown in Figs. 3(e) and 3(f). Briefly, we performed four additional scans with the SPAD positioned at ±25° and ±45° angles from the optical axis, and the image reconstruction was performed using the randomized algebraic reconstruction technique with 500 iterations [5] and a 0.5 mm × 0.5 mm grid. Jacobians were computed with TR-MC. The image obtained with EPs allowed significantly better separation of targets, although more noise was observed in the image due to reduced SNR at early times. Although the relationship between narrower PDSFs and resolution has been clearly established previously [2–5], measurement noise is also an important consideration, and development of algorithms to mitigate these effects are ongoing. For example, we recently described a method for joint use of early and CW photons in image reconstruction to trade off resolution and quantitative accuracy [5].

In summary, in combination with a Ti:sapphire laser, the SPAD was extremely effective in measurement of EPs and yielded the narrowest EP PDSFs that we have been able to measure to date (i.e., a reduction of 63%–68% versus the CW case). For example, this is in contrast to ~50% reduction in PDSF width in our previous work [6] where the overall system TIRF was 163 ps. Most significantly, EP PDSF measurements were close to the theoretical limit defined by TR-MC over the early time gates considered (~1% of peak or later), which we have not been able to achieve previously. In the context of DOT, potential disadvantages of this detector type include the "diffusion tail" effect [Fig. 1(c)], which distorts the decay portion of the TR curve, and the relatively small detector area (~50 μm × 50 μm), which limits the overall sensitivity.

Characterization of EP DOT imaging performance with SPADs is ongoing, and we next plan to build a small animal EP imager using multiple detectors. We have also not yet tested the SPAD in measurement of fluorescence, which is typically of several orders of magnitude lower intensity than the excitation light.

This work was funded with a grant from the National Institutes of Health (R01EB012117).

References

1. S. R. Arridge, Inverse Probl. **15**, R41 (1999).
2. S. Andersson-Engels, R. Berg, S. Svanberg, and O. Jarlman, Opt. Lett. **15**, 1179 (1990).
3. J. Wu, L. Perelman, R. R. Dasari, and M. S. Feld, Proc. Natl. Acad. Sci. USA **94**, 8783 (1997).
4. V. Venugopal, J. Chen, F. Lesage, and X. Intes, Opt. Lett. **35**, 3189 (2010).
5. Z. Li and M. Niedre, Biomed. Opt. Express **2**, 665 (2011).
6. N. Valim, J. Brock, M. Leeser, and M. Niedre, Phys. Med. Biol. **58**, 335 (2013).
7. F. Stuker, C. Baltes, K. Dikaiou, D. Vats, L. Carrara, E. Charbon, J. Ripoll, and M. Rudin, IEEE Trans. Med. Imaging **30**, 1265 (2011).
8. A. Tosi, A. D. Mora, F. Zappa, A. Gulinatti, D. Contini, A. Pifferi, L. Spinelli, A. Torricelli, and R. Cubeddu, Opt. Express **19**, 10735 (2011).
9. M. J. Niedre, G. M. Turner, and V. Ntziachristos, J. Biomed. Opt. **11**, 064017 (2006).